Journal of Modern Optics
Publication details, including instructions for authors and subscription information:
http://www.tandfonline.com/loi/tmop20

Diffraction by Cantor fractal zone plates

J. A. Rodrigo [a] , T. Alieva [a] , M. L. Calvo [a] & J. A. Davis [b]
[a] Departamento de Óptica, Facultad de Ciencias Físicas , Universidad Complutense de Madrid , 28040 Madrid, Spain
[b] San Diego State University, Department of Physics , San Diego, CA 92182-1233, USA
Published online: 19 Aug 2006.

To cite this article: J. A. Rodrigo , T. Alieva , M. L. Calvo & J. A. Davis (2005) Diffraction by Cantor fractal zone plates, Journal of Modern Optics, 52:18, 2771-2783, DOI: 10.1080/09500340500356973

To link to this article: http://dx.doi.org/10.1080/09500340500356973

Journal of Modern Optics
Vol. 52, No. 18, 15 December 2005, 2771–2783

Diffraction by Cantor fractal zone plates

J. A. RODRIGO*†, T. ALIEVA†,
M. L. CALVO† and J. A. DAVIS‡
†Departamento de Óptica, Facultad de Ciencias Físicas,
Universidad Complutense de Madrid, 28040 Madrid, Spain
‡San Diego State University, Department of Physics,
San Diego, CA 92182-1233, USA

(*Received 5 April 2005; in final form 13 September 2005*)

The paper reports studies, both experimental and using numerical simulation, of the Fresnel diffraction by recently introduced fractal zone plates associated with triadic and quintic Cantor sets. The evolution of the intensity patterns at planes transversal to the propagation direction is presented. A series of conventional and doughnut-like foci are observed around the principal focus. The position, depth and size of the foci depend on similarity dimensions and the fractal level of the encoded fractal structures, both directly related to the number of the corresponding Fresnel zones.

1. Introduction

After the introduction by Mandelbrot [1] two decades ago of the concept of fractal geometry, the research on light interaction with fractals objects and the discovery of fractal features of electromagnetic fields resulted in the development of fractal electrodynamics and fractal optics [2–4]. Therefore it is useful to analyse the diffraction in these types of fractal gratings. Theoretical and experimental research on Fraunhofer and Fresnel diffraction by deterministic and random fractals has been done [5–11]. Moreover, it has been shown that some optical fields have an intrinsic fractal structure [12, 13]. In previous research the authors [9] studied diffraction by particular gratings that exhibit a fractal structure in the domain of positional coordinates. Nevertheless, the fractal behaviour can be observed with respect to other parameters such as the square of the positional coordinates. This domain is of interest in optics since it is related to the Fresnel zone domain.

Recently, fractal zone plates (ZPs) with a fractal structure along the square of the transverse coordinates have been introduced [14–18]. These zone plates differ from conventional Fresnel zone plates that have a periodic structure along the square of the transverse coordinates. The focusing properties of the two-dimensional fractal ZPs for the case of triadic Cantor set modulation have been analytically studied [15].

*Corresponding author. Email: jarmar@fis.ucm.es

Journal of Modern Optics
ISSN 0950–0340 print/ISSN 1362–3044 online © 2005 Taylor & Francis
http://www.tandf.co.uk/journals
DOI: 10.1080/09500340500356973

In particular it has been shown, theoretically, that the intensity distribution along the optical axis as a function of Fresnel number for the fractal ZP, exhibits fractal behaviour. In a previous paper [17], the authors implemented for the first time, triadic Cantor ZPs in a liquid-crystal display. The predicted focusing properties were observed.

In this paper we consider not only the intensity distribution along the optical axis, but we analyse as well the whole observation plane and the evolution of the diffraction patterns as a function of the longitudinal coordinate z. In this study we have discovered a peculiar property of the Cantor ZPs to focus light in the form of doughnut-like structures.

This paper is organized as follows. First we discuss the Fresnel diffraction by circular zone plates and the structure of particular class of fractal ZPs, the so-called Cantor ZPs. In sections 3 and 4 we analyse the evolution of the intensity distribution of the field diffracted by the triadic and quintic Cantor ZPs and the corresponding Fresnel ZPs, considering a series of variable values for the propagation distance, up to the position at which the far field operates In section 5 the previous results obtained by numerical simulation are verified experimentally by encoding the Cantor ZP onto an amplitude transmittance film. Finally, we discuss the findings and present conclusions in section 6.

2. Background

Let us consider the diffraction of a monochromatic plane wave by a rotationally symmetric zone plate with amplitude transmittance $p(r_0)$. The intensity distribution of the diffraction pattern at the parallel plane $I(r, z)$ situated at a distance z from the zone plate plane and considering the Fresnel approximation is given by

$$I(r,z) = \left(\frac{2\pi}{\lambda z}\right)^2 \left| \int_0^a p(r_0) \exp\left(i\frac{\pi}{\lambda z} r_0^2\right) J_0\left(\frac{2\pi r r_0}{\lambda z}\right) r_0 dr_0 \right|^2, \tag{1}$$

where a is the radius of the ZP pupil function and λ is the wavelength of the incoming light. The purpose of this paper is to study the evolution of diffraction intensity patterns $I(r, z)$ for the case of fractal ZPs as a function of the arbitrary propagation distance z.

In particular, the intensity distribution along the z axis ($r = 0$) is described as

$$I(0,z) = \left(\frac{2\pi}{\lambda z}\right)^2 \left| \int_0^a p(r_0) \exp\left(i\frac{\pi}{\lambda z} r_0^2\right) r_0 dr_0 \right|^2. \tag{2}$$

For convenience we introduce new variables (the same as in [15]): $s = (r_0/a)^2 - 0.5$; $q(s) = p(r_0)$ and $u = a^2/2\lambda z$, we obtain:

$$I(0,u) = 4\pi^2 u^2 \left| \int_{-0.5}^{0.5} q(s) \exp(i2\pi u s) ds \right|^2. \tag{3}$$

For the particular fractal zone plate generated as a Cantor fractal structure and defined in [14–18], the associated function $q(s)$ exhibits fractal behaviour. In contrast,

$q(s)$ is a periodic function for the case of the conventional Fresnel zone plate. For the fractal ZP from the family of the Cantor sets considered in this paper, $q(s)$ is generated applying an iterative procedure by dividing the initial segment into the $2N-1$ segments and eliminating the segments in the even positions. Then, after a number S of iterations, we obtain a modulated Fresnel ZP exhibiting fractal structure. The number S defines the so called fractal level, giving an idea of the complexity of the fractal object. The number of the Fresnel zones of the corresponding conventional Fresnel ZP is $(2N-1)^S$.

In this paper, we study the diffraction by the triadic ($N=2$) and quintic ($N=3$) Cantor ZPs of levels $S=2$ and $S=3$. The fractal self-similarity dimensions of triadic and quintic Cantor sets, used for the Cantor ZP construction, are readily calculated by applying the standard definition: $D_S=\log N/\log(1/R)$, where N is the order of the fractal (the number of segments is $2N-1$) and R the reduction factor, then we obtain: $\log 2/\log 3$ and $\log 3/\log 5$, correspondingly [20].

The position of the principal focus is determined by the radius of the first Fresnel zone of the ZP. Therefore, to preserve the position of the principal focus for zone plates of various fractal level and dimension, we have to vary the outer radius $a_{S,N}$ of the ZP pupil function according to the type of zone plate. In order to compare the numerical simulation and our experimental results we have chosen a radius for the first Fresnel zone of $a_0=0.96\,\text{mm}$ that corresponds to focal length of $f=(a_0)^2/\lambda=1.45\,\text{m}$. Consequently, the outer radius $a_{S,N}$ takes the following values for the fractal and Fresnel zone plates (figure 1):

Triadic Cantor ZP of level $S=2$ and Fresnel ZP with 9 zones, $a_{2,2}=2.88\,\text{mm}$.
Triadic Cantor ZP of level $S=3$ and Fresnel ZP with 27 zones, $a_{3,2}=4.99\,\text{mm}$.
Quintic Cantor ZP of level $S=2$ and Fresnel ZP with 25 zones, $a_{2,3}=4.8\,\text{mm}$.
Quintic Cantor ZP of level $S=3$ and Fresnel ZP with 125 zones, $a_{3,3}=10.73\,\text{mm}$.

3. Axial intensity distribution

In order to study the evolution of the diffracted field we are interested in defining the axial intensity distribution. For the case of the Cantor ZPs, the intensity distribution along the optical axis ($r=0$) can be written [15] as a function of the normalized variable u as

$$I_{CZP}(0,u,N,S)=4\sin^2\left[\frac{\pi u}{(2N-1)^S}\right]\prod_{k=1}^{S}\frac{\sin^2\left[2\pi Nu/(2N-1)^k\right]}{\sin^2\left[2\pi u/(2N-1)^k\right]}, \tag{4}$$

where S is the level of the fractal structure (number of iterations used to generate $q(s)$) and N characterizes the different Cantor sets. It is easy to see that $I_{CZP}(0,u,N,S)$ is a periodic function of u with period $(2N-1)^S$. The principal maximum inside the period (we consider u from the interval $[0,(2N-1)^S]$) is located at the position $u=(2N-1)^S/2$. Meanwhile as the fractal level increases, new hole points (with zero intensity at $r=0$) and secondary maxima of the intensity appear along the optical axis in a particular sequence determined by the self-similarity dimensions.

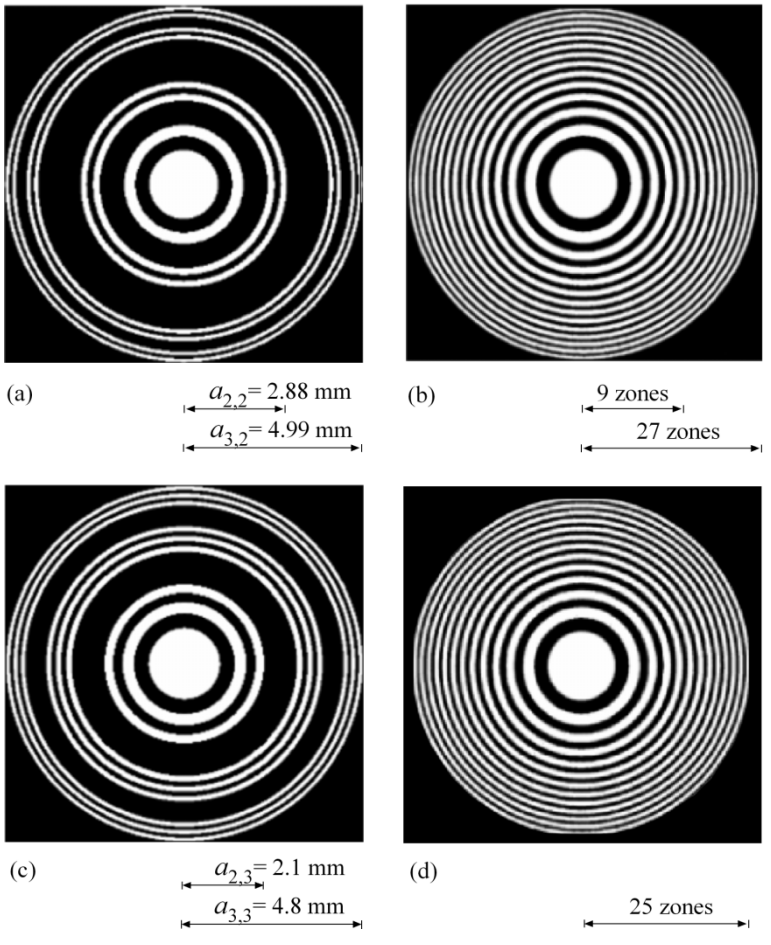

Figure 1. Triadic Cantor ZP of level $S=3$ (a) and the associated Fresnel ZP (b). Quintic Cantor ZP of level $S=2$ (c) and the associated Fresnel ZP (d). a_s is the pupil radius corresponding to the fractal ZP of level S.

For the case of the corresponding Fresnel zone plate, the intensity distribution as a function of the Fresnel numbers can be written in the form:

$$I_{FZP}(0,u,N,S)=\frac{\sin^2\left(\left(2\pi u/(2N-1)^S\right)M\right)}{\cos^2\left(\pi u/(2N-1)^S\right)}, \tag{5}$$

where $M=\text{integer}((2N-1)^S/2)+1$. Note that $I_{FZP}(0,u,N,S)$ is also a periodic function of u. Its period and position of the principal maximum remain the same as for $I_{CZP}(0,u,N,S)$. The focused peaks form at positions corresponding to $z=f, f/3, f/5$ etc.

For practical applications, we note that the focusing properties (focal lengths, intensities, depth and size of the focused spots) are the main parameters for zone plate characterization.

Based on equations (4) and (5), but representing the intensity distributions $I_{CZP}(0, z, N, S)$ and $I_{FZP}(0, z, N, S)$ as a function of propagation distance z, we have performed a comparative analysis of focus properties of the triadic ($N=2$) and quintic ($N=3$) Cantor ZPs of different levels, and the corresponding Fresnel ZPs. For practical reasons we limit ourselves to a region around the principal focus since the regions around $f/3$, $f/5$ demonstrate similar behaviour but with some scaling.

In figure 2 the intensity distribution along the optical axis for triadic Cantor ZPs $I_{CZP}(0, z, 2, S)$ (b) and the associated Fresnel ZPs $I_{FZP}(0, z, 2, S)$ (a) are shown. Figure 2(a) shows that, as the aperture of the ZP increases, the focus sharpens along the axial direction. Figure 2(b) shows two effects. First as the order of the fractal increases, the number of focus spots increases. Second, because the aperture increases as the fractal order increases, each of these peaks becomes more sharply focused along the axial direction.

The arrows in figure 2(b) indicate the distances of experimentally observed secondary foci and hole points (zero intensity) for the triadic Cantor ZP of level 3, which will be discussed in section 5.

Figure 3 shows analogous results for the quintic Cantor and Fresnel ZPs where $N=3$. In both cases, the dotted curves correspond to $S=2$ and the continuous curves correspond to $S=3$. We notice various facts: figure 3(a) again shows that, as the aperture of the ZP increases, the focus sharpens along the axial direction. Figure 3(b) shows two effects as well. First as the order of the fractal increases, the number of focus spots increases. Second, because the aperture increases as the fractal order increases, each of these peaks becomes more sharply focused along the axial direction. By comparing figures 2(b) and 3(b), we see that the number of focus spots increases as the S parameter increases. The axial intensity distributions corresponding to the ZPs of low level involve the curves of the upper ones. As the fractal level increases, the number of focal points increases and the number of secondary foci and hole points at the optical axis increases as well. We also note that the depth of focus along the axial direction decreases as the fractal level increases for all of the principal and secondary foci. This occurs because the aperture size increases as the fractal order increases as discussed earlier.

We also note that the Cantor and Fresnel ZPs defined by the same N and S have almost the same depth of the principal focus. The depth decreases with increasing N or S; this is equivalent to increasing the number of Fresnel zones. Then, we conclude that the depth of the principal focus depends on the number of Fresnel zones (by parameter a) of the ZPs. Thus, for example, the depth of the principal focus of the triadic Cantor ZP of level 3 – the number of corresponding Fresnel zones is 27 – (see continuous curve in figure 2b) is almost the same as one of the principal focus of the quintic Cantor ZP of level 2 – the number of corresponding Fresnel zones is 25 – (see dotted curve in figure 3b) indicating that some similarities are obtained with various types of fractal ZPs.

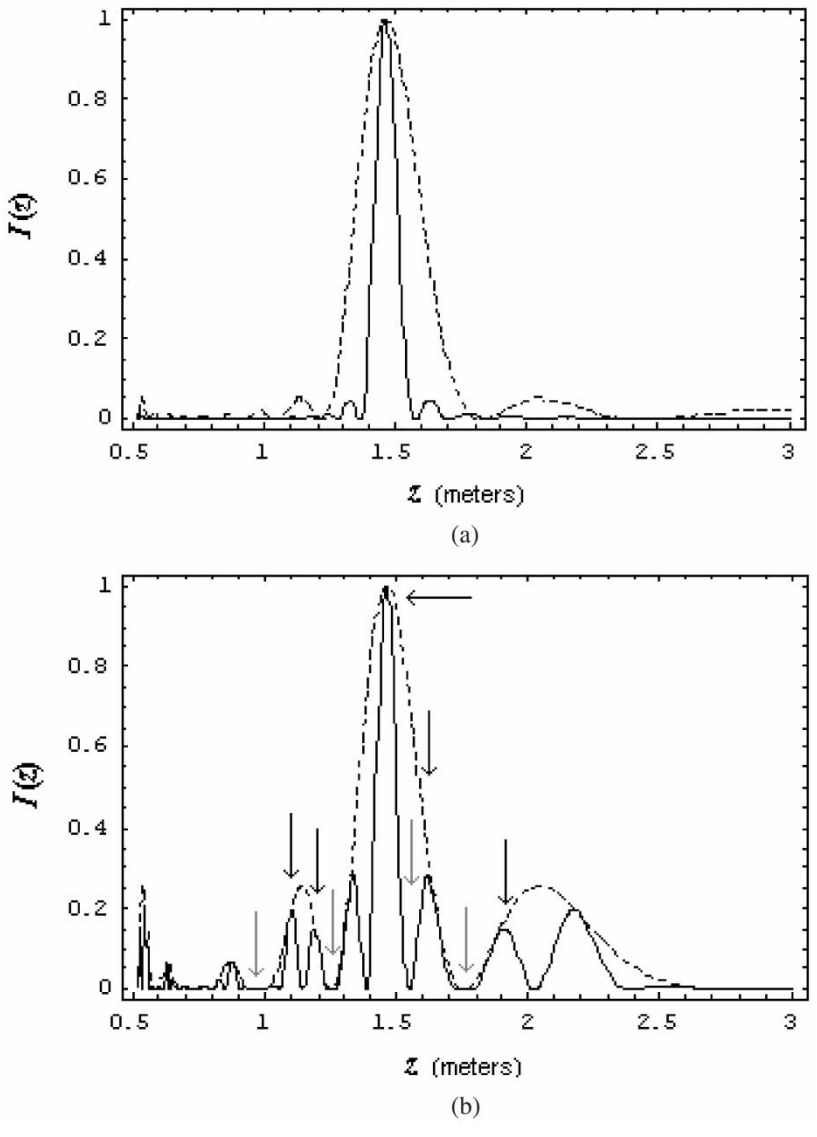

Figure 2. Intensity distribution along the z axis for (a) Fresnel ZPs ($N=2$): $S=2$ (- - - - -) and $S=3$ (—), (b) triadic Cantor ZPs ($N=2$): $S=2$ (- - - - -) and $S=3$ (—). Note: Arrows indicate hole points and foci experimentally observed.

4. Structure of diffraction patterns for Cantor zone plates: numerical study

Let us now consider the evolution of the intensity profiles, taken along the diameter (r-coordinate), of the optical field diffracted by the Cantor and corresponding Fresnel ZPs with the distance z. For that we utilize the so-called propagation tree or bifurcation levels, from which it is possible to observe if there is a hierarchical

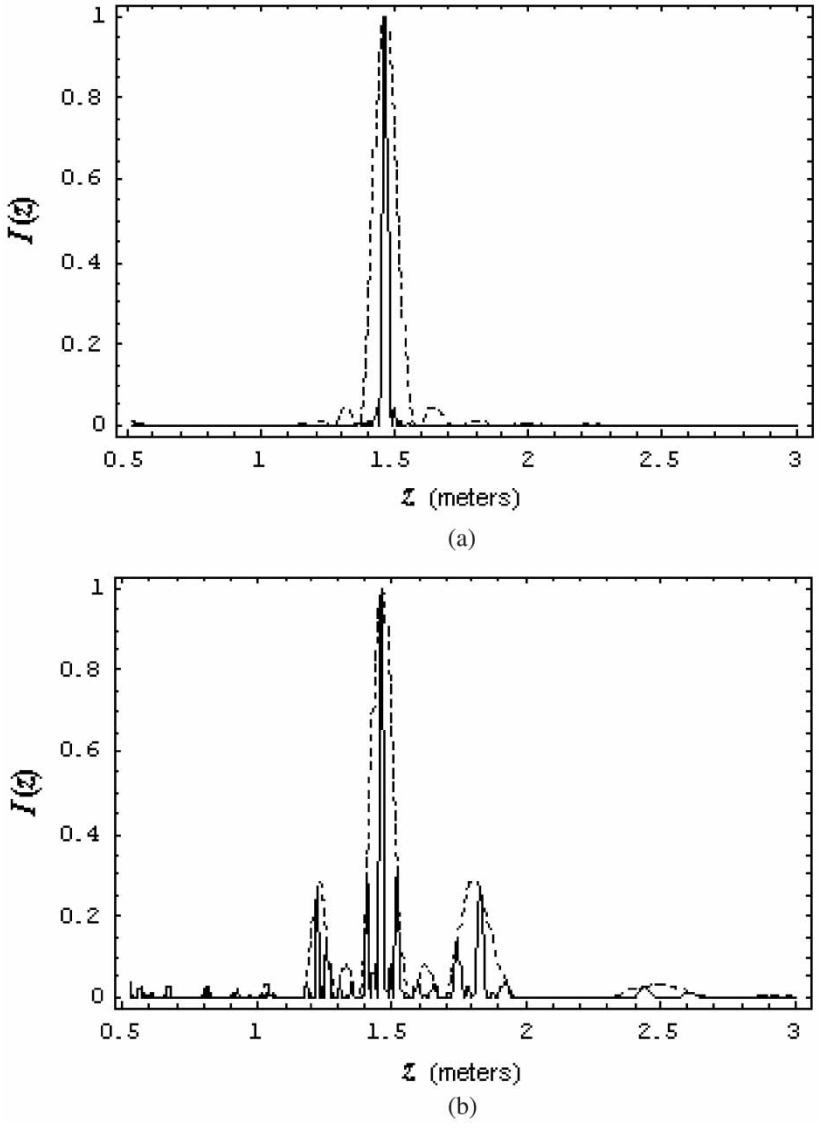

Figure 3. Intensity distribution along the z-axis (a) Fresnel ZPs [$N=3$]: $S=2$ (- - - - -) and $S=3$ (—) (b) quintic Cantor Fractal ZPs [$N=3$]: $S=2$ (- - - - -) and $S=3$ (—).

structure on the propagation law associated to the fractal tree. The diffraction patterns have been obtained by applying an algorithm developed by us for the Fresnel regime and based upon the convolution theorem [22, 23].

In figures 4 and 5 we compare the evolution of the intensity profiles within a range of 3 m of propagation and 1 cm of transversal section. The intensity is represented in a grey scale, as a function of the distance z for the triadic Cantor

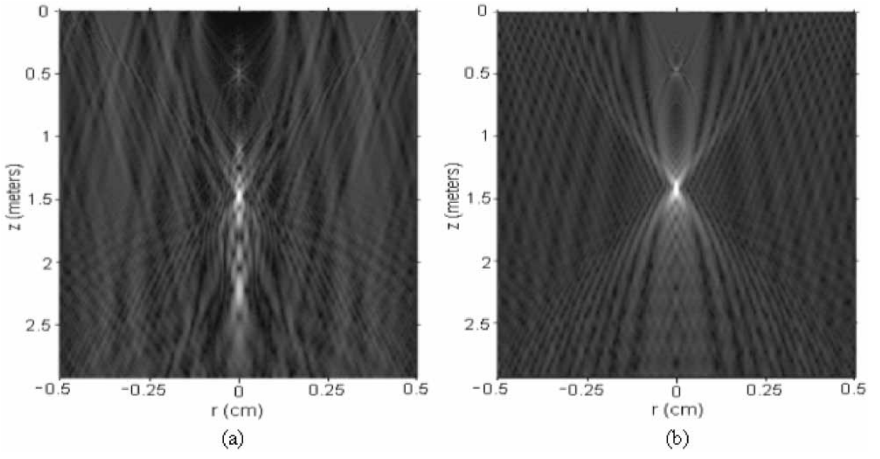

Figure 4. Evolution of the intensity profiles corresponding to triadic Cantor ZP [$N=2$, $S=3$] (a), and associated Fresnel ZP (b) obtained by means of numerical simulation.

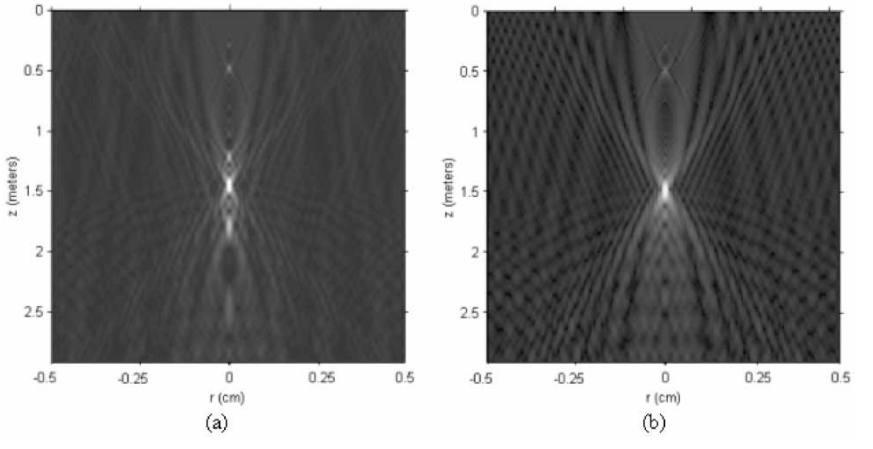

Figure 5. Evolution of the intensity profiles corresponding to quintic Cantor ZP [$N=3$, $S=2$] (a), and associated Fresnel ZP (b) obtained by means of numerical simulation.

ZP $I_{CZP}(r,z,2,3)$ of level 3 (figure 4a), the quintic Cantor ZP $I_{CZP}(r,z,3,2)$ of level 2 (figure 5a) and the associated Fresnel zone plates $I_{FZP}(r,z,2,3)$ (figure 4b) and $I_{FZP}(r,z,3,2)$ (figure 5b), respectively. In each case the intensity distributions were calculated for the diffraction of the plane monochromatic wave ($\lambda=632.8$ nm) and zone plates with pupil radii that correspond to our experimental conditions as discussed in section 2.

Note that for the conventional Fresnel ZPs (figures 4b and 5b) both diffraction trees have self-affine structure related to the existence of several focal points. Thus we can distinguish three regions located around the focal points $z=f=1.45$ m, $z=f/3$ and $z=f/5$ which are similar.

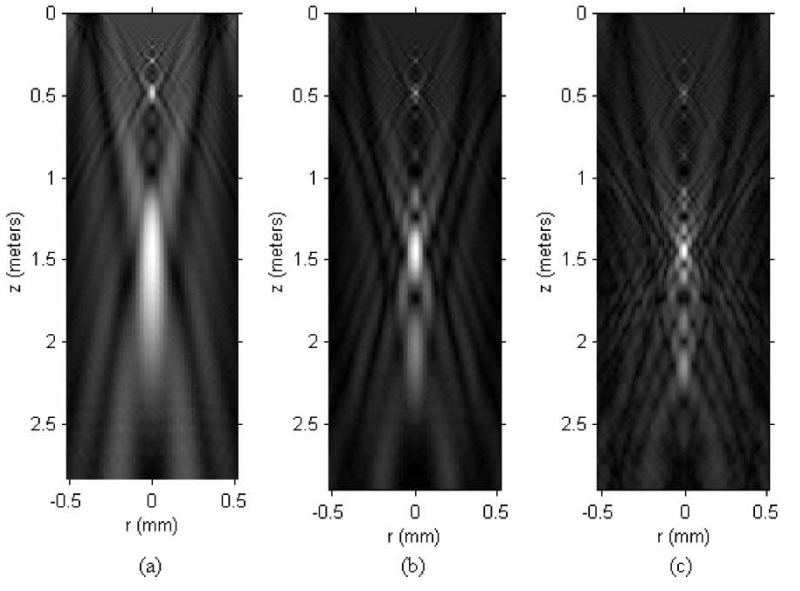

Figure 6. Evolution of the intensity profiles corresponding to triadic Cantor ZPs [$N=2$] for $S=1$ (a), $S=2$ (b), and $S=3$ (c) obtained by means of numerical simulation.

The intensity distributions for the fractal ZPs in figures 4(a) and 5(a) exhibit the complex structure inside each of these regions, defining a chain-like structure which can be better seen around the principal focus. In addition to the secondary fractal foci, doughnut-like structures with zero intensity at the optical axis are observed (see also figure 2). The doughnut-like structures are seen at the corresponding distances in the form of a radial maximum concentrated around the hole.

In figure 6, the diffraction trees for the triadic Cantor ZPs of different levels $S=1$, figure 6(a), $S=2$ figure 6(b), $S=3$ figure 6(c) are displayed. We stress that the depth of the foci decrease as the level S increases, since more Fresnel zones participate in their formation, so that the chain-like structure is less defined for low fractal level.

5. Experimental results

For experimental verification of the previous numerically simulated results we have assembled a set-up as shown in figure 7. A collimated beam illuminates the object plane where we located a fractal ZP with the amplitude transmittance of the triadic Cantor ZP of level 3 and the quintic Cantor ZP of level 2, generated on the PC (256×256 pixels) and further printed on the corresponding transparency with resolution 600 dpi. The diameter of the pupil function is 1 cm. The collimated coherent monochromatic light interacts with the fractal ZP and the diffracted pattern is registered by a CCD camera at the different propagation distances.

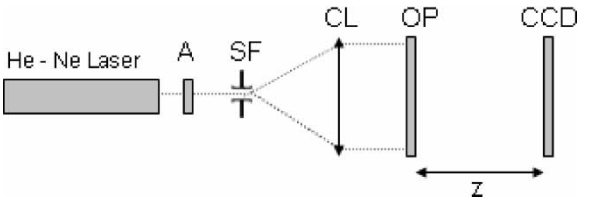

Figure 7. Experimental set up, where A is an attenuator, SF–spatial filter, CL–collimating lens ($f = 1$ m), OP is the object plane, z variable distance of free propagation, and CCD camera.

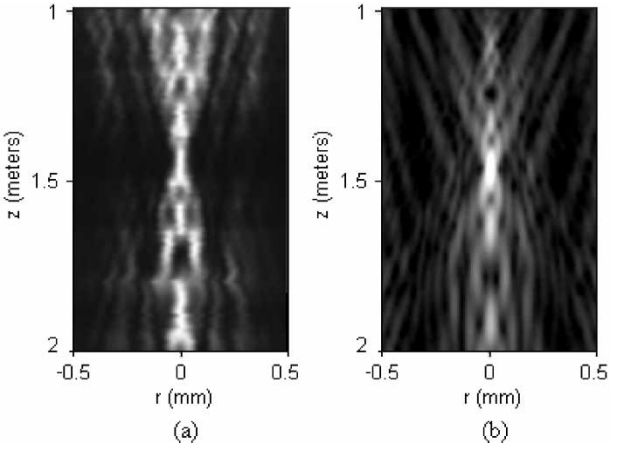

Figure 8. The comparison of the diffraction trees for triadic Cantor ZPs [$S = 3$, $N = 2$] obtained experimentally (a) and by means of numerical simulation (b). Notice that experimental main focus is saturated in order to enhance the contributions of the secondary foci.

In our experiments we use He–Ne laser ($\lambda = 632.8$ nm) with 10 mW of output power, and a Hamamatsu ORCA-285 CCD camera.

We have studied the Fresnel diffraction by the Cantor ZPs in the region around the principal focus (section of 1 cm). By displacing the CCD camera along the optical axis in the region from 0.52 m to 2 m with a step of 1 cm, we obtain a sequence of 148 diffraction patterns for both the considered cases of triadic Cantor ZP [$N = 2$, $S = 3$] and quintic Cantor ZP [$N = 3$, $S = 2$]. We perform the diffraction tree so that from every diffraction pattern we select a section fitting the length of the diameter of the ZP, so that the thickness of each section corresponds to one pixel of the CCD camera (6 μm in the actual case). Then, placing them consecutively in growing order of z, we build up the image representing a part of the diffraction tree of triadic Cantor ZP (figure 8a) and quintic Cantor ZP (figure 9a), respectively. In figures 8(b) and 9(b) the corresponding numerical simulation of the diffraction trees of similar resolution are shown. The grey scale indicates the intensity levels. The diffraction trees constructed from the experimental data (see figures 8a and 9a), depict the main

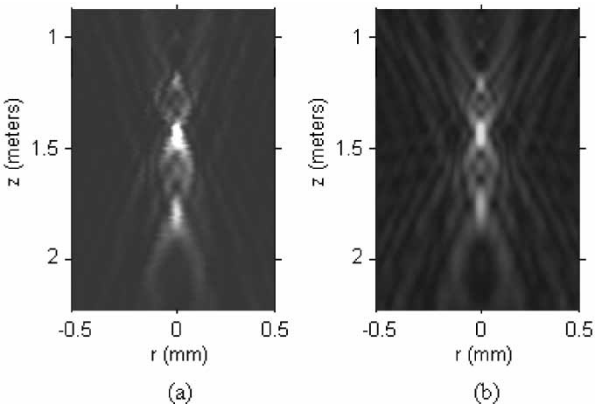

Figure 9. Comparison of the diffraction trees for quintic Cantor ZPs [$S = 2$, $N = 3$] obtained experimentally (a) and by means of numerical simulation (b).

features of the diffraction tree calculated numerically. Experimental results are in reasonable agreement with theory.

Considering again the results in figure 2(b), one notices that secondary foci around the principal one (indicated by the arrows) have been observed in our experiments. Some of the corresponding images of the diffraction patterns on triadic Cantor ZP, are displayed identically as they were recorded in the experiments (transverse to the propagation plane) in figure 10(b), (c), (e), (g) and (i), respectively.

The experimental diffraction patterns corresponding to the doughnut-like intensity distribution are shown in figure 10(a), (d), (f) and (h). The foci and doughnut-like structures are also observed for the quintic Cantor ZP.

The size of the secondary focus spot and the radius of the doughnut-like focus and their depth depend on their position z. The size and the depth of secondary foci and doughnut-like structures located after the principal one are more extended than their symmetrical counterparts located in front of it. The minimal diameter (the distance between two intensity peaks) of the doughnut-like structure observed in the experiment is about 0.32 mm. It is located at the distance $z = 1.24$ m (see figure 10d).

6. Discussion and conclusions

The properties of standard Fresnel zone plates are very well known now, having been studied for several decades [21]. Nevertheless, the study of modified Fresnel zone plates obtained by including in their structure fractal behaviour is not yet well covered in the literature nor have their possible applications been widely exploited. This is mainly due to the difficulties in obtaining good quality experimental fractal ZPs since high resolution is required to demonstrate their major features. We have studied the focusing properties of the fractal Cantor ZPs both

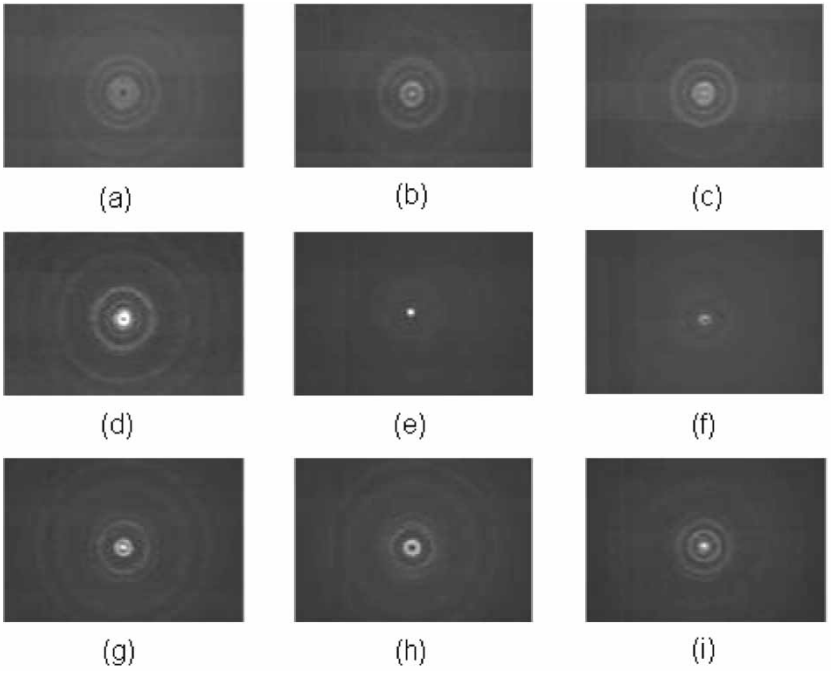

Figure 10. Experimental diffraction patterns corresponding to distances (a) $z = 0.97$ m, (b) $z = 1.12$ m, (c) $z = 1.17$ m, (d) $z = 1.24$ m, (e) $z = 1.45$ m, (f) $z = 1.57$ m, (g) $z = 1.62$, (h) $z = 1.71$ m, and (i) $z = 1.92$ m.

numerically and experimentally. We have shown that the number of the secondary foci depends on the fractal levels and fractal self-similarity dimensions. The size and the depth of the secondary foci are defined by the number of Fresnel zones in the associated Fresnel ZP. The experimental results for the case of a triadic Cantor ZP of level 3 and quintic Cantor ZP of level 2 are in good agreement with numerical simulations, indicating the feasibility of these particular ZPs.

In addition to the spot foci, we found doughnut-like structures with zero intensity distribution at the optical axis. The size and depth of the doughnut-like structures depend on their position at the optical axis. Some of the experimentally observed doughnut-like structures have radius $0.032a$, where a is the pupil radius of the ZP. At this point we have to add that chain-like structures in which one can observe the formation of sequences of doughnut-like zones and secondary foci are not exclusively observed with fractal ZPs. From results not displayed here for brevity [19] such beams have been generated in other modulated zone plates. However, the interest in pursuing the present study is related to the particular sequences and moreover to the distribution of the diffracted energy, not only in the axial direction but over the whole transverse plane. Thus a two-dimensional analysis is required. Further research has to be devoted to the possible applications of these fractal Cantor ZPs.

Acknowledgements

Research supported by projects TIC2002-1846 and TIC2002-11581-E Ministerio de Educación y Ciencia, Spain. T. Alieva acknowledges receipt of a ''Ramón y Cajal'' grant from Ministerio de Educación y Ciencia, Spain. The authors acknowledge the technical support of Hamamatsu (R. Diaz) in providing the CCD camera for these experiments.

References

[1] B.B. Mandelbrot, *The Fractal Geometry of Nature* (Freeman, San Francisco, CA, 1982).
[2] M.V. Berry, J. Phys. A: Math. Gen. **12** 781 (1979).
[3] C. Allian and M. Cloitre, Phys. Rev. B **33** 3563 (1986).
[4] J. Uozumi and T. Asakura, in *Current Trends in Optics*, edited by J.C. Dainty (Academic Press, Cambridge, MA, 1994), pp. 83–94.
[5] D.L. Jaggard and X. Sun, J. Opt. Soc. A **7** 1131 (1990).
[6] Y. Sakurada, J. Uozumi and T. Asakura, Pure Appl. Opt. **3** 371 (1994).
[7] T. Alieva and F. Agullo-Lopez, Opt. Commun. **125** 267 (1996).
[8] M. Lehman, Opt. Commun. **195** 11 (2001).
[9] D. Rodriguez Merlo, J.A. Rodrigo Martín-Romo, T. Alieva, and M.L. Calvo, Opt. Spectrosc. **95** 131 (2003).
[10] T. Alieva and M.L. Calvo, J. Opt. A: Pure and Appl. Opt. **5** S324 (2003).
[11] L. Zunino and M. Garavaglia, J. Mod. Opt. **50** 717 (2003).
[12] G.P. Karman and J.P. Woerdman, Opt. Lett. **23** 1909 (2001).
[13] M.V. Berry and S. Klein, J. Mod. Opt. **43** 2139 (1996).
[14] D. Calva Méndez and M. Lehman, SPIE Proc. **4829** 309 (2002).
[15] G. Saavedra, W.D. Furlan and J.A. Monsoriu, Opt. Lett. **28** 971 (2003).
[16] J.A. Monsoriu, G. Saavedra and W.D. Furlan, Opt. Express, **12** 4227 (2004).
[17] J.A. Davis, L. Ramirez, J.A. Rodrigo, T. Alieva and M.L. Calvo, Opt. Lett. **29** 1321 (2004).
[18] J.A. Rodrigo, T. Alieva, M.L. Calvo and J.A. Davis, in *Integrated Optical Devices, Nanostructures, and Displays*, edited by K.L. Lewis, Proc. SPIE, Vol. 5622 (Venezuela, 2004), p. 1474.
[19] M.L. Calvo, J. Rodrigo and T. Alieva, Proc. ICO-20, Proc. SPIE on CD-ROM, Vol. 6027 (paper 0403-028).
[20] H. Peitgen, H. Jürgens and D. Saupe, *Chaos and Fractals* (Springer, New York, 1992), p. 205.
[21] J. Ojeda-Catañeda and C. Gómez-Reino (Eds), *Selected Papers on Zone Plates* (SPIE Optical Engineering Press, Washington, 1996).
[22] D. Mendlovic, Z. Zalevsky and N. Konforti, J. Mod. Opt. **44** 407 (1997).
[23] D. Mas, J. Garcia, C. Ferreira, L.M. Bernardo and F. Marinho, Opt. Commun. **164** 233 (1999).